Effect of Assembly Stiffness and Solder Properties on Thermal Cycle Acceleration Factors

Robert Darveaux[1,2]

[1]Amkor Technology, Inc
1900 S. Price Rd.
Chandler, AZ 85248

[2]Arizona State University at the Polytechnic Campus
Department of Electronics and Computer Engineering Technology
College of Technology and Applied Science
Mesa, AZ

ABSTRACT

The impact of assembly stiffness and solder properties on thermal cycle acceleration factors was investigated using a simplified model of an electronic assembly. It was seen that stress – strain hysteresis loops change dramatically with modest changes in assembly stiffness or imposed strain. The impact on strain range or strain energy density saturates as the assembly stiffness significantly exceeds that of the solder.

The acceleration factors between various temperature cycle conditions vary with assembly stiffness and solder properties. Hence, standard qualification tests do not accelerate all types of surface mount components equally. Strain energy density appears to be a more robust damage indicator than strain range, based on its lower sensitivity to specific constitutive relations.

1. INTRODUCTION

Reliability prediction models have several important uses: 1) optimization of a product design before it is manufactured, 2) optimization of a product after it has already failed a qualification test, 3) estimation of field use reliability, and 4) establishing appropriate accelerated tests based on the field use conditions. In the case of solders used in electronic packaging, fatigue life under cyclic loading conditions is typically correlated to strain range per cycle [1-10,23] or strain energy density per cycle [8,10-20,23].

In all predictive models, accurate calculation of the stresses and strains in the solder joint is critical. In order to perform a structural calculation, constitutive models are needed which describe the relationship between stress, strain, strain rate, temperature, and microstructure. There are several forms of constitutive relations for solders in use today (see for example refs [15,20-25]).

Product qualification generally takes a different approach. The industry has established a series of qualification tests over the years, and each new generation of product is expected to pass the same number of cycles as the previous generation. In some cases, companies will relax certain criteria over time, but they are always reluctant due to liability concerns over field returns.

For example, temperature cycle qualification for cellular phone applications has traditionally been 1000 cycles - 40C⇔125C, with 15min ramps, 15min dwells. Over time, this has been reduced in some cases to 300 to 600 cycles (although the "target" is still 1000 cycles). In order to make such a reduction, it is necessary to have a good understanding of the acceleration factors between the qualification test conditions and the field use conditions. In general, these acceleration factors will depend on both the assembly stiffness and the solder properties.

The present paper explores the interaction of assembly stiffness and solder properties with respect to thermal cycle acceleration factors. A 1-dimensional mechanical model is used for the analysis. Three solder alloys are compared: 62Sn36Pb2Ag, 97.5Pb2.5Sn, and 96.5Sn3.5Ag. The properties of these alloys are representative of those being used in various flip chip, BGA, and SMT applications. In all simulations, both the inelastic strain range and the total strain energy density are used as damage indicators to predict fatigue life.

2. SIMPLIFIED MODEL OF AN ELECTRONIC ASSEMBLY

The mechanical model used in the present analysis is shown schematically in Figure 1. There are 4 elements which represent (1) the elastic response of the assembly, (2) the elastic response of the solder, (3) the time-

independent plastic flow response of the solder, and (4) the time and temperature dependent creep response of the solder. When the assembly undergoes a temperature change, it is represented by an imposed strain on the system. Methods to estimate the assembly stiffness and imposed strain are discussed in refs [3,26]

For example, in moving from the "initial" condition to the "ramp" condition in Figure 1, the assembly and solder springs stretch, and the solder undergoes both plastic flow and creep. The net strain of these 4 elements is equal to the imposed strain on the system. The relative magnitude of these effects depends on the stiffness of the assembly and solder elements, and on the plastic flow and creep properties for the solder.

During the "dwell" condition in Figure 1, the assembly and solder springs contract and the creep deformation of the solder increases. The overall strain is held fixed, and the stress relaxes. The magnitude of this stress relaxation depends on the stiffness of the assembly and solder elements, and on the creep properties of the solder.

After the dwell, the imposed strain is applied in the opposite direction. It is assumed that the solder recovers during the dwell, and the plastic flow and primary creep behavior start again from zero, i.e., there is no cyclic work hardening. Evidence of this effect is given in Refs [27,28].
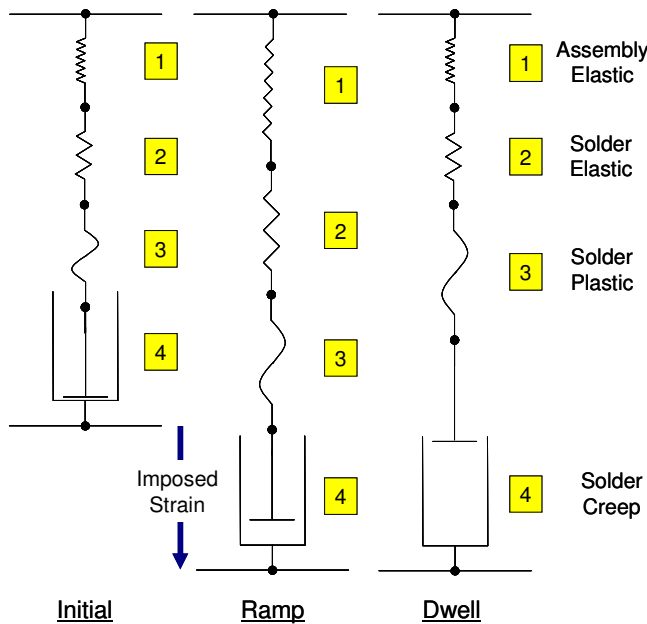

Figure 1. Simplified Model of an Electronic Assembly

3. CONSTITUTIVE RELATIONS FOR SOLDER

The constitutive relations for the solder used in the present study were taken from refs [15,25]. The inelastic solder properties were measured on BGA joints loaded in shear. The values were then converted to equivalent tensile constants.

The elastic modulus is given by

$$E = E_O - E_1(T-273) \qquad (1)$$

where E_O is the modulus at 273K, T is the absolute temperature, and E_1 gives the temperature dependence.

The steady state (or minimum) creep rate is given by

$$\frac{d\varepsilon_S}{dt} = C_{SS}[\sinh(\alpha\sigma)]^n \exp(\frac{-Q_a}{kT}) \qquad (2)$$

where $d\varepsilon_S/dt$ is the steady state strain rate, k is Boltzmann's constant, σ is the applied stress, Qa is the apparent activation energy, n is the stress exponent, α prescribes the stress level at which the power law dependence breaks down, and C_{SS} is a constant.

Steady state creep is not generally achieved immediately when stress is applied. A certain amount of primary creep occurs before attaining steady state. For normal decelerating primary creep, the strain rate starts high and decreases to a minimum value as the material work hardens. The instantaneous creep rate at constant stress and temperature is given by

$$\frac{d\varepsilon_c}{dt} = \frac{d\varepsilon_S}{dt}(1+\varepsilon_T B \exp(-B\frac{d\varepsilon_S}{dt}t)) \qquad (3)$$

where $d\varepsilon_c/dt$ is the instantaneous creep rate, ε_T is the transient creep strain, and B is the transient creep coefficient.

In addition to time dependent creep, some time independent plastic flow can occur in solders at high stresses. The following strain hardening law was used to describe time independent plastic flow

$$\varepsilon_p = C_p\sigma^m \qquad (4)$$

where ε_p is the time-independent plastic strain, and C_p and m are constants.

The elastic strain is calculated by Hook's law

$$\varepsilon_e = \sigma/E \qquad (5)$$

The total strain is given by the sum of elastic strain, creep strain, and plastic strain

$$\varepsilon_t = \varepsilon_e + \varepsilon_c + \varepsilon_p \qquad (6)$$

where ε_t is the total strain.

The constitutive constants for the 3 solder alloys used in the present analysis are given in Table 1.

Table 1. Constitutive constants for 3 solder alloys.

Parameter	96.5Sn3.5Ag	97.5Pb2.5Sn	62Sn36Pb2Ag
E_o (Mpsi)	7.6	3.5	5.1
E_1 (Kpsi/K)	27	4.1	22
C_{ss} (1/sec)	1.42e5	2.66e11	8.03E4
α (1/psi)	3.64e-4	4.63e-4	4.62e-4
n	5.5	7.0	3.3
Qa (eV)	0.75	1.15	0.70
ε_T	0.096	0.066	0.023
B	227	237	263
C_p (psi^{-m})	1.20e-18	8.16e-15	1.19E-23
m	4.39	3.10	5.53

4. THERMAL CYCLE ACCELERATION FACTORS

An acceleration factor is defined as the number of cycles to failure under field use conditions relative to accelerated test conditions.

$$AF = N_{field} / N_{acc\ test} \qquad (7)$$

For a given joint size, solder fatigue is generally found to be inversely proportional to strain energy density to the power j. Hence when comparing 2 different thermal cycle conditions, the acceleration factor is given by

$$AF_{1,2} = (\Delta W_2 / \Delta W_1)^j \qquad (8)$$

where $AF_{1,2}$ is the ratio of fatigue life for temperature cycle condition 1 versus condition 2, and ΔW is the strain energy density accumulated per cycle. The exponent, j, is typically found to be close to 1 [8,10-20,23].

When using inelastic strain range as the failure indicator, it is typically found that the fatigue life is inversely proportional to the strain range to the k power. Hence the acceleration factor between two temperature cycle conditions is given by

$$AF_{1,2} = (\Delta\varepsilon_2 / \Delta\varepsilon_1)^k \qquad (9)$$

where $\Delta\varepsilon$ is the inelastic strain range. The exponent k is found to be in the range of 1 to 2 [1-10,23].

In the present study, five different temperature cycle conditions were considered, as shown in Table 2. Profile #1 is a typical package level qualification test. Profiles #3 and #4 are typically used in board level qualification studies. Profile #5 is meant to represent a field use condition for a computing application.

Table 2
Simulated Thermal Cycle Profiles

Profile	Low Temp (C)	High Temp (C)	Ramp Time (sec)	Dwell Time (sec)
1	-55	125	180	720
2	-55	125	720	180
3	-40	125	900	900
4	0	100	600	300
5	25	75	600	13800

Shown in Figure 2 is a typical stress – strain hysteresis loop generated by stepping through time and solving for the stress and strain at each time increment. The stress is considered to represent equivalent normal stress, but the positive and negative signs have no real meaning in the current context. In general, solder will be under shear + compressive stress on one side of the temperature cycle and shear + tensile stress on the other side. Whether tensile occurs on the hot or cold side of the chamber depends on the location in a joint and on the specifics of the assembly structure and expansion mismatches.

The inelastic strain range and strain energy density are defined in Figure 2. Notice that the inelastic strain range is not equal in both directions. This is called thermal ratcheting, and it results in a net change in joint shape with cycling (see for example refs [9,29]. The inelastic strain energy density is the area within the hysteresis loop. In the present study, the total strain energy density (which includes the elastic component) will be used to calculate acceleration factors. It was found in ref [30] that <u>total</u> strain energy density gave a better correlation than <u>inelastic</u> strain energy density for cyclic bending tests that lasted between 10,000 and 100,000 cycles.

Subsequent work has shown that total strain energy density per cycle also correlates well to thermal cycle fatigue data that is in the range of 100 to 10,000 cycles.
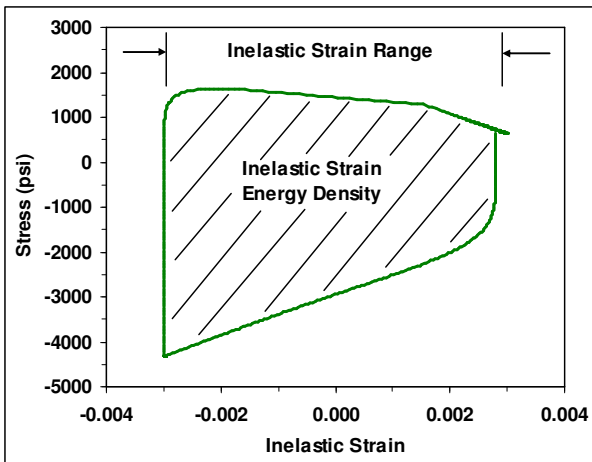

Figure 2. Stress – inelastic strain hysteresis loop for 96.5Sn3.5Ag, Temperature cycle condition 3 (-40C⇔125C, 900 sec ramps, 900 sec dwells), 5.E5 psi assembly stiffness, 1.E-4/C imposed strain.

5. EFFECT OF ASSEMBLY STIFFNESS AND IMPOSED STRAIN

The impact of increasing assembly stiffness on stress – strain hysteresis loops is shown in Figure 3. With all other factors held constant, it is seen that the peak stresses, the strain range, and the strain energy density all increase dramatically with increases in assembly stiffness.

In BGA assemblies, things that increase stiffness are double sided assemblies and increasing motherboard thickness, die thickness, and mold cap thickness. Reducing the pad area and the number of solder joints also increases the effective assembly stiffness compared to the joint array. In leaded assemblies, the lead design is a key parameter, in addition to the factors discussed above for BGAs. See refs [16,30-32] for examples on how measured fatigue life was reduced by such increases in assembly stiffness.

The effect of increasing imposed strain is shown in Figure 4. With all other factors held constant, it is seen that the peak stresses, the strain range, and the strain energy density all increase dramatically with increases in imposed strain. A 4X increase in imposed strain results in an 8X increase in inelastic strain range due to the highly non-linear nature of the solder constitutive relations.

Factors that affect the imposed strain in a structure are die size, package size, joint height, and expansion mismatches

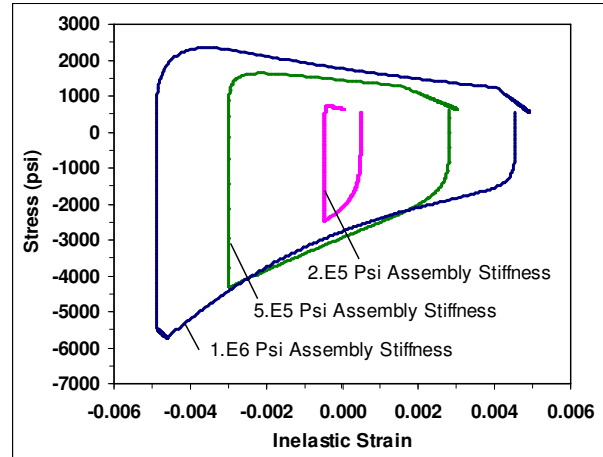between the materials. There are numerous examples in the literature showing these effects.

Figure 3. Stress – inelastic strain hysteresis loops for 96.5Sn3.5Ag, Temperature cycle condition 3 (-40C⇔125C, 900 sec ramps, 900 sec dwells), 1.E-4/C imposed strain.
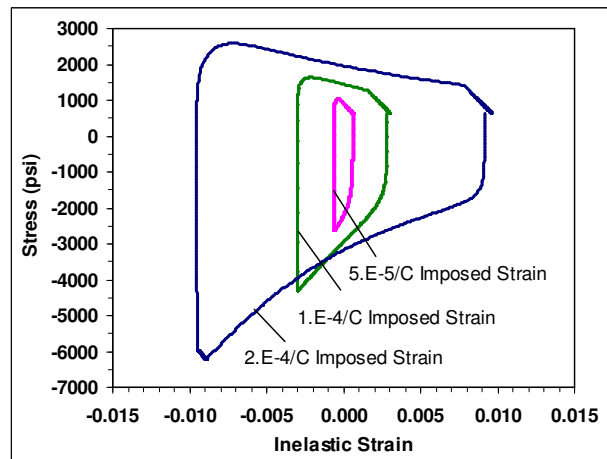

Figure 4. Stress – inelastic strain hysteresis loops for 96.5Sn3.5Ag, Temperature cycle condition 3 (-40C⇔125C, 900 sec ramps, 900 sec dwells), 5.E5 psi assembly stiffness.

A contour map showing how strain energy density per cycle is impacted by combinations of assembly stiffness and imposed strain is shown in Figure 5. For a given level of imposed strain, the strain energy density increases rapidly with stiffness, then starts to saturate at a maximum value. Saturation occurs as the stiffness of the assembly becomes significantly greater than the stiffness of the solder.

A contour plot for inelastic strain range is shown in Figure 6, which demonstrates similar trends to Figure 5.
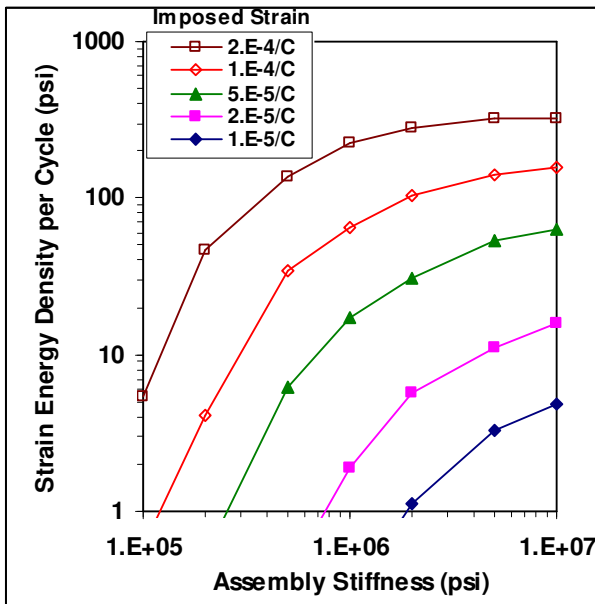
Figure 5. Strain energy density per cycle for 96.5Sn3.5Ag under temperature cycle condition 1 (-55C⇔125C, 180 sec ramps, 720 sec dwells).
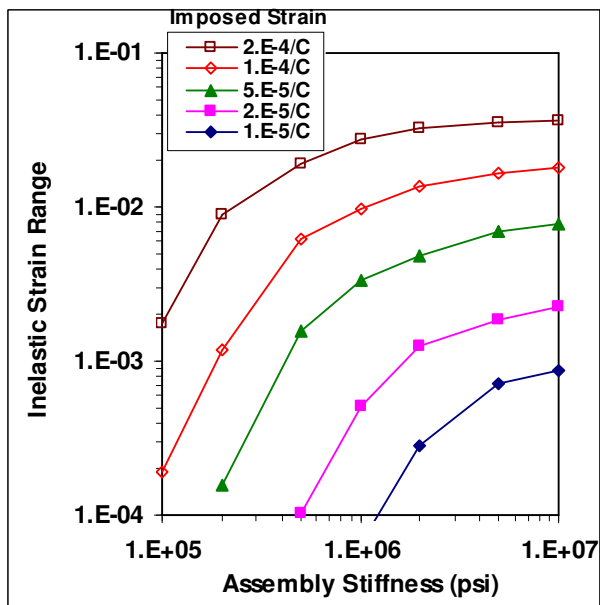

Figure 6. Inelastic strain range for 96.5Sn3.5Ag under temperature cycle condition 1 (-55C⇔125C, 180 sec ramps, 720 sec dwells).

6. INTERACTION OF TEMPERATURE CYCLE CONDITIONS AND SOLDER PROPERTIES

The impact of assembly stiffness on strain energy density and inelastic strain range is shown in Figures 7 – 12 for

five temperature cycle conditions and three alloys. The imposed strain was 1.E-4/C for all simulations. It is seen that there is a rapidly increasing portion to the curves, followed by a saturation portion as the assembly stiffness becomes greater than the solder stiffness.

The vertical separation between curves in these figures varies with stiffness. This indicates that the acceleration factor between two different thermal cycle conditions will also vary with assembly stiffness. In some regimes the acceleration factor is increasing with stiffness, and in other regimes it is decreasing.

This has important ramifications for product qualification. Typically, the exact same tests are used to do board level qualification of different components in a product. Since the effective assembly stiffness for the various components will be different, the equivalent number of field use years will also be different.

In comparing the strain energy density plots (Figures 7,9,11) to the strain range plots (Figures 8,10,12) it is seen that different acceleration factors will be predicted depending on the damage indicator. For example, the simulations for 62Sn36Pb2Ag show that for assembly stiffness less than 5.E5 psi, TC #5 is more damaging than TC #4 if inelastic strain range is considered (Figure 8). On the other hand, the opposite trend is predicted if strain energy density is used as the damage indicator (Figure 7).

Furthermore, a measurable difference in fatigue life is expected between temperature cycle profiles #1, #2, and #3 when considering strain energy density. However, curves for these conditions are virtually convergent when considering inelastic strain range.

Plots comparing the three alloys with respect to strain energy density per cycle are shown in Figures 13 and 14. It is seen that the trend with assembly stiffness is slightly different for each alloy under TC #1 conditions. However, the differences are much greater between alloys under TC #5 conditions. Hence, the acceleration factors between qualification and field use conditions will be alloy dependent.

This effect is shown more clearly in Figures 15 and 16, where the fatigue life ratio is estimated using strain energy density and inelastic strain range, respectively. An imposed strain of 1.E-4/C was used in the simulations. Again, the acceleration factor depends on alloy, stiffness, and damage indicator. The largest discrepancies between alloys are in the stiffness range of 5.E5 psi and below. Also, inelastic strain range will predict a larger variation between alloys than strain energy density.

A comparison in fatigue life ratio between TC#1 and TC#2 is shown in Figures 17 and 18. These conditions have the same temperature range and cyclic frequency, but vary in the ramp times and dwell times. A traditional Norris-Landsberg approach would predict the exact same

life for both of these conditions (ratio = 1). The fatigue life ratio based on strain energy density is alloy and stiffness dependent and it varies from 0.95 to 1.25. If one considers inelastic strain range, the predicted life ratio is generally closer to 1, but still depends on alloy and stiffness.
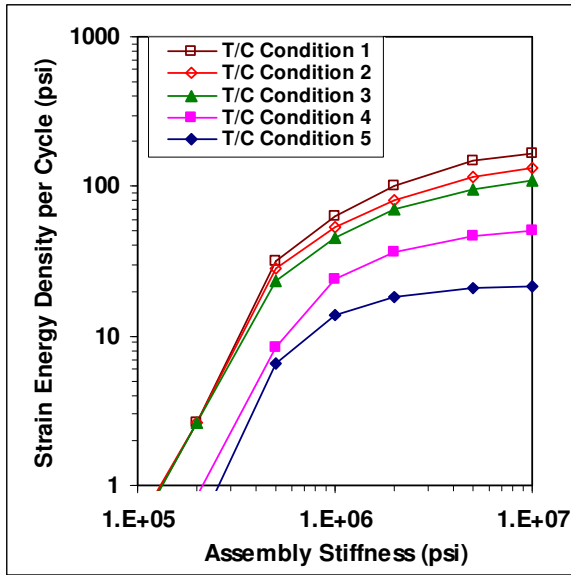
Figure 7. Strain energy density per cycle for 62Sn36Pb2Ag under various temperature cycle conditions, 1.E-4/C imposed strain.
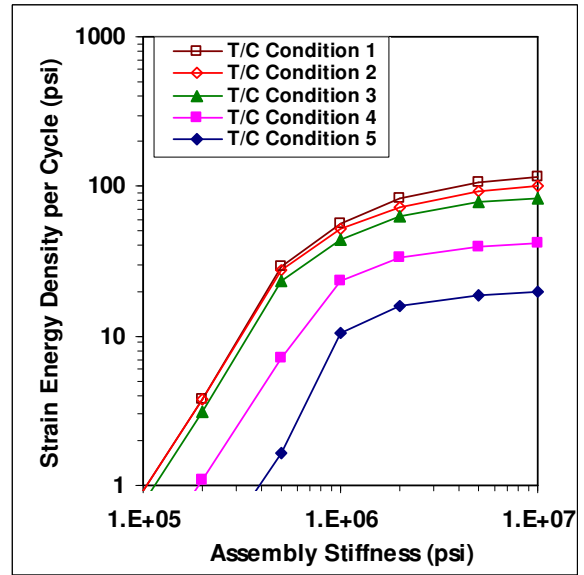
Figure 9. Strain energy density per cycle for 97.5Pb2.5Sn under various temperature cycle conditions, 1.E-4/C imposed strain.
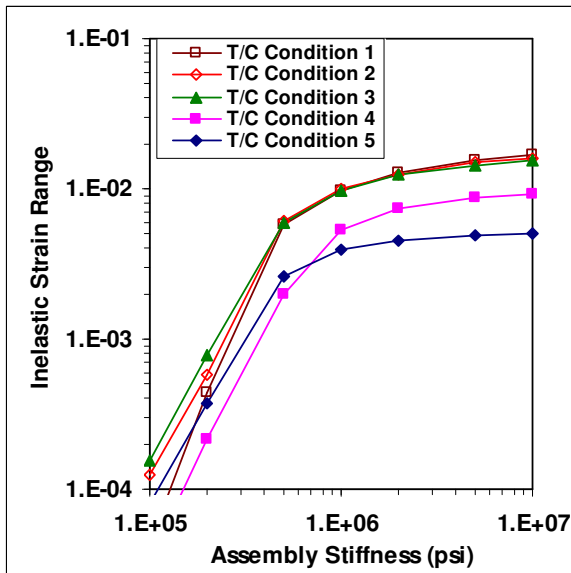
Figure 8. Inelastic strain range for 62Sn36Pb2Ag under various temperature cycle conditions, 1.E-4/C imposed strain.
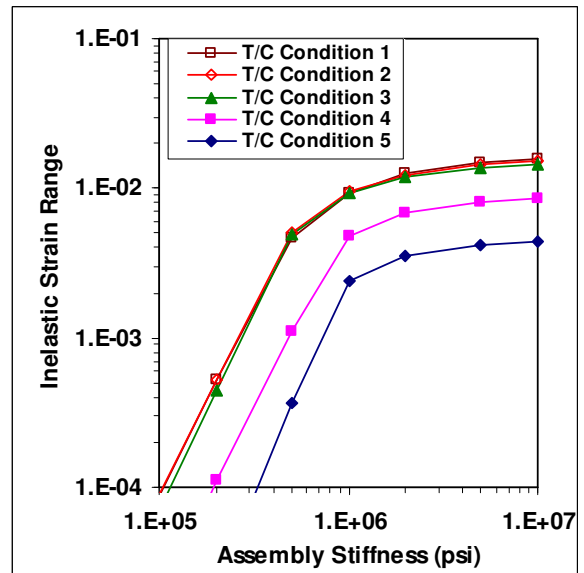

Figure 10. Inelastic strain range for 97.5Pb2.5Sn under various temperature cycle conditions, 1.E-4/C imposed strain.
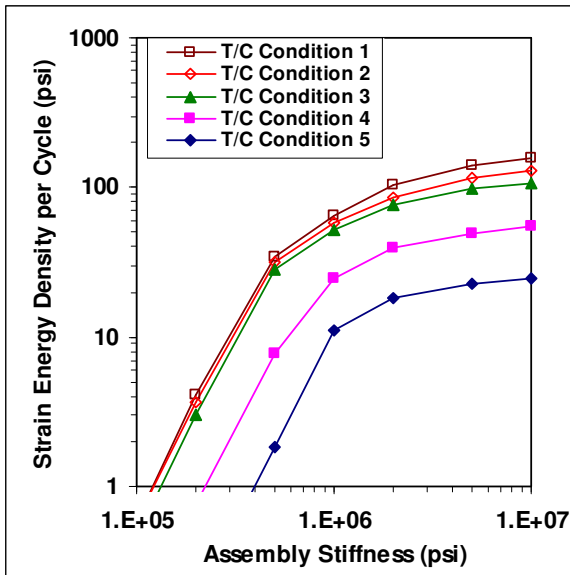
Figure 11. Strain energy density per cycle for 96.5Sn3.5Ag under various temperature cycle conditions, 1.E-4/C imposed strain.
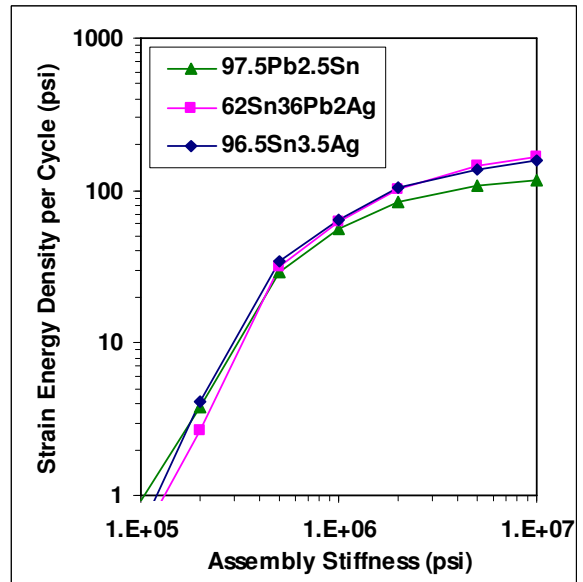

Figure 13. Comparison of strain energy density per cycle for three alloys, temperature cycle condition 1 (-55C⇔125C, 180sec ramps, 720 sec dwells), 1.E-4/C imposed strain.
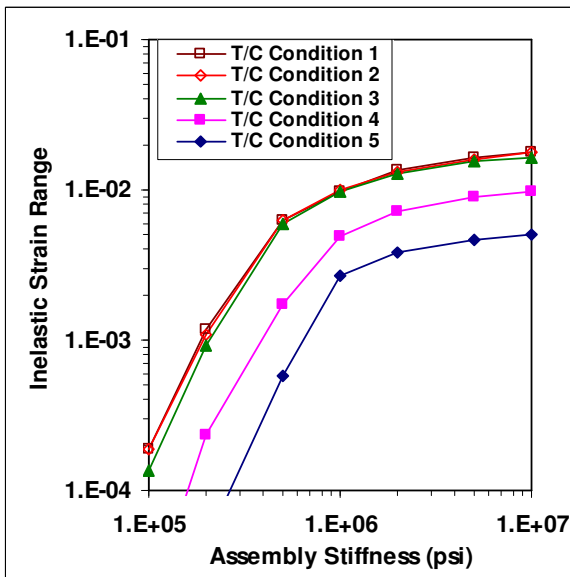

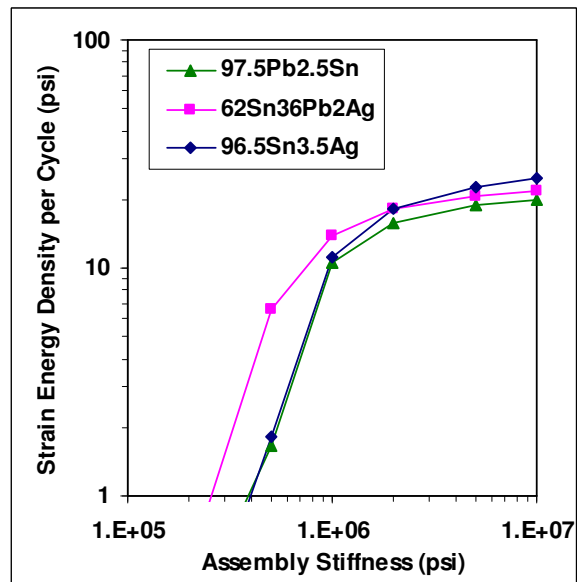Figure 12. Inelastic strain range for 96.5Sn3.5Ag under various temperature cycle conditions, 1.E-4/C imposed strain.

Figure 14. Comparison of strain energy density per cycle for three alloys, temperature cycle condition 5 (25C⇔75C, 600sec ramps, 13800 sec dwells), 1.E-4/C imposed strain.
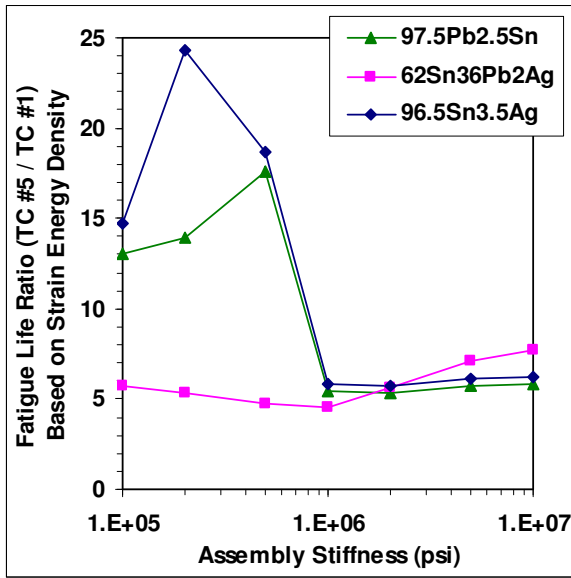
Figure 15. Fatigue life ratio based on (Strain Energy Density)$^{-1}$ for temperature cycle condition 1 (-55C⇔125C, 180 sec ramps, 720 sec dwells) vs. condition 5 (25C⇔75C, 600 sec ramps, 13800 sec dwells), 1.E-4/C imposed strain.
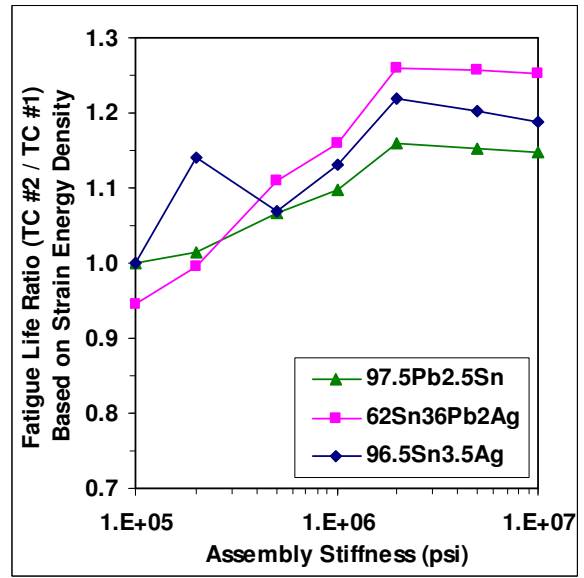

Figure 17. Fatigue life ratio based on (Strain Energy Density)$^{-1}$ for temperature cycle condition 1 (-55C⇔125C, 180 sec ramps, 720 sec dwells) vs. condition 2 (-55C⇔125C, 720 sec ramps, 180 sec dwells), 1.E-4/C imposed strain.

Figure 16. Fatigue life ratio based on (Inelastic Strain Range)$^{-2}$ for temperature cycle condition 1 (-55C⇔125C, 180 sec ramps, 720 sec dwells) vs. condition 5 (25C⇔75C, 600 sec ramps, 13800 sec dwells), 1.E-4/C imposed strain.

Figure 18. Fatigue life ratio based on (Inelastic Strain Range)$^{-2}$ for temperature cycle condition 1 (-55C⇔125C, 180 sec ramps, 720 sec dwells) vs. condition 2 (-55C⇔125C, 720 sec ramps, 180 sec dwells), 1.E-4/C imposed strain.
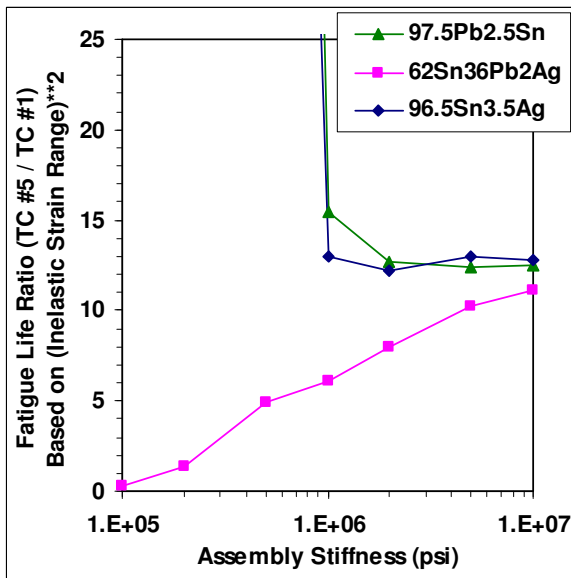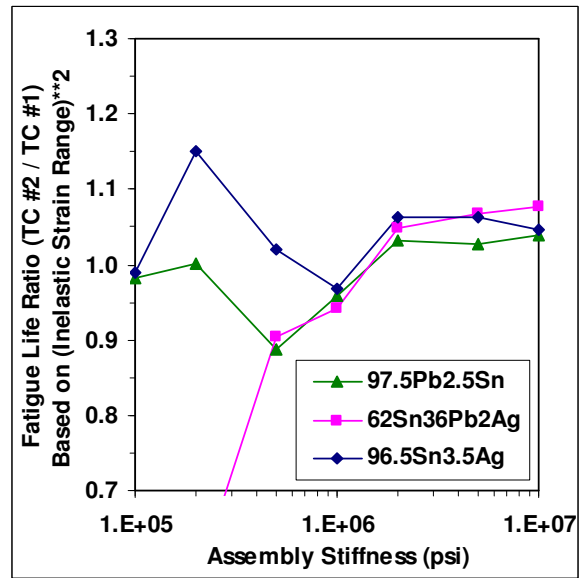
7. EFFECT OF CONSTITUTIVE RELATIONS

The inelastic constitutive relations used in this study include time independent plastic flow, primary creep, and steady state creep. As discussed previously, there are several versions of constitutive relations being used in the industry to predict solder fatigue. A common practice is to only use steady state creep, since it is most conveniently available in finite element software. Also, there is rather large variation in the measured material constants depending on the investigators sample configuration and test method (see ref [34] for more discussion).

Shown in Figure 19 are stress-strain hysteresis loops using progressively more complex constitutive relations. It is seen that only using steady state creep results in the largest stress range, but the smallest strain range. Adding primary creep, and then plastic flow progressively reduces the predicted stress range and increases the strain range.

The effect of constitutive relations on strain energy density and inelastic strain range is shown for the three alloys in Figures 20 - 25. In all cases the imposed strain was 1.E-4/C.

In the stiffness range greater than 1.E6 psi, using only steady state creep tends to over-predict the strain energy density per cycle. At lower assembly stiffness, the strain energy density is under predicted. Using only steady state creep always under-predicts the inelastic strain range.
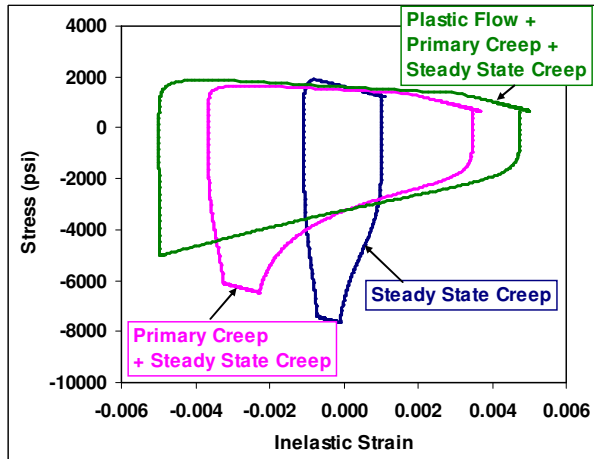

Figure 19. Stress – Strain hysteresis loops for 96.5Sn3.5Ag solder with various constitutive models, temperature cycle condition 3 (-40C⇔125C, 900 sec ramps, 900 sec dwells), 4.0E5 psi assembly stiffness, 1.5E-4/C imposed strain.

Adding plastic flow becomes important in the low stiffness regime for 97.5Pb2.5Ag and 96.5Sn3.5Ag solders. In general, the calculated strain energy density is less sensitive to constitutive relations than inelastic strain range is.
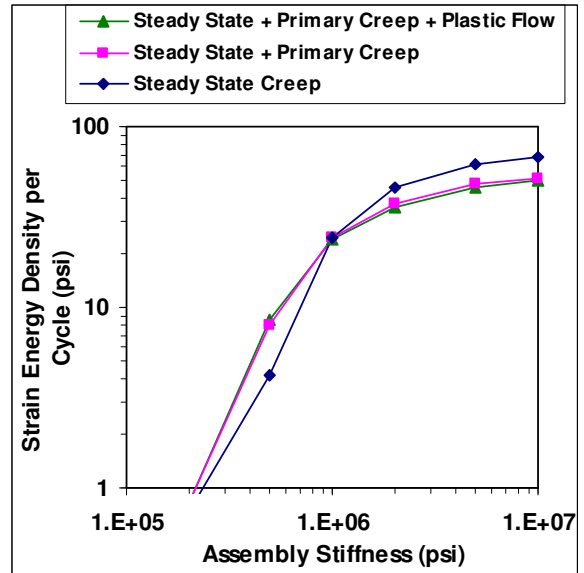

Figure 20. Effect of constitutive relations on Strain Energy Density per cycle for 62Sn36Pb2Ag solder under temperature cycle condition 4 (0C⇔100C, 600 sec ramps, 300 sec dwells) and 1.0E-4/C imposed strain.

Figure 21. Effect of constitutive relations on Inelastic Strain Range for 62Sn36Pb2Ag solder under temperature cycle condition 4 (0C⇔100C, 600 sec ramps, 300 sec dwells) and 1.0E-4/C imposed strain.

Figure 22. Effect of constitutive relations on Strain Energy Density per cycle for 97.5Pb2.5Sn solder under temperature cycle condition 4 (0C⇔100C, 600 sec ramps, 300 sec dwells) and 1.0E-4/C imposed strain.

Figure 24. Effect of constitutive relations on Strain Energy Density per cycle for 96.5Sn3.5Ag solder under temperature cycle condition 4 (0C⇔100C, 600 sec ramps, 300 sec dwells) and 1.0E-4/C imposed strain.

Figure 23. Effect of constitutive relations on Inelastic Strain Range for 97.5Pb2.5Sn solder under temperature cycle condition 4 (0C⇔100C, 600 sec ramps, 300 sec dwells) and 1.0E-4/C imposed strain.
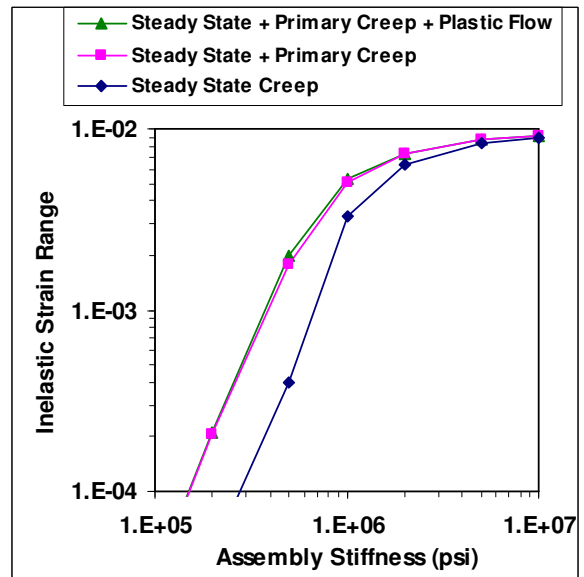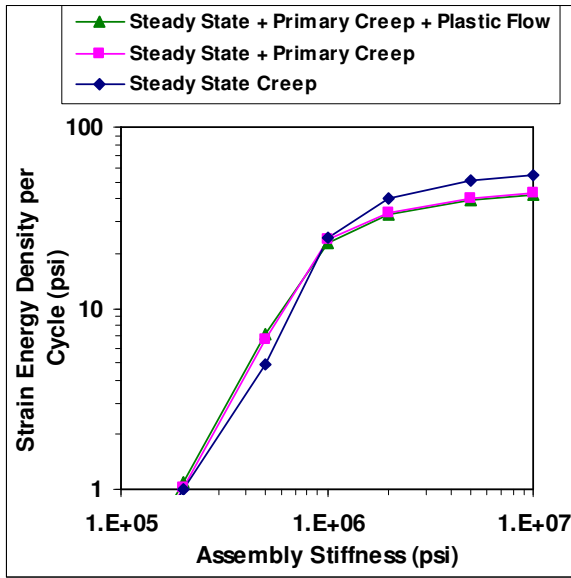

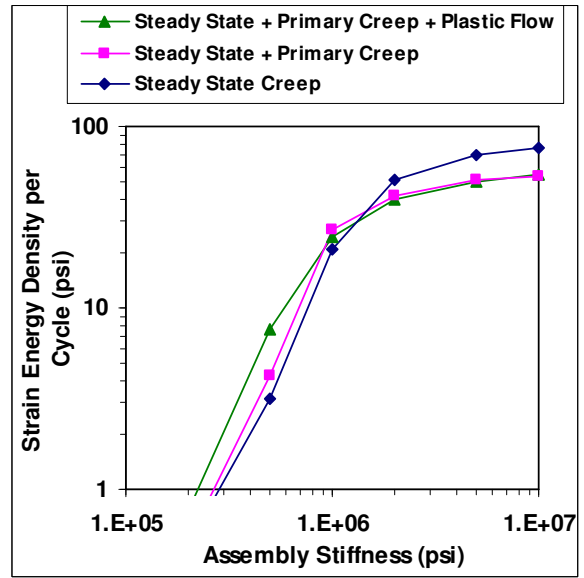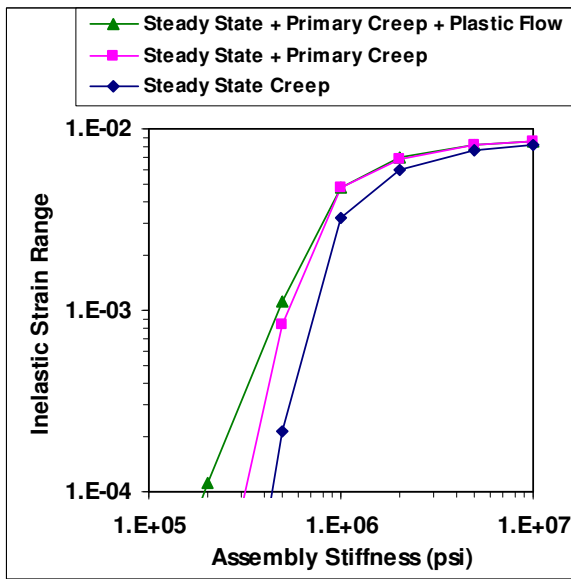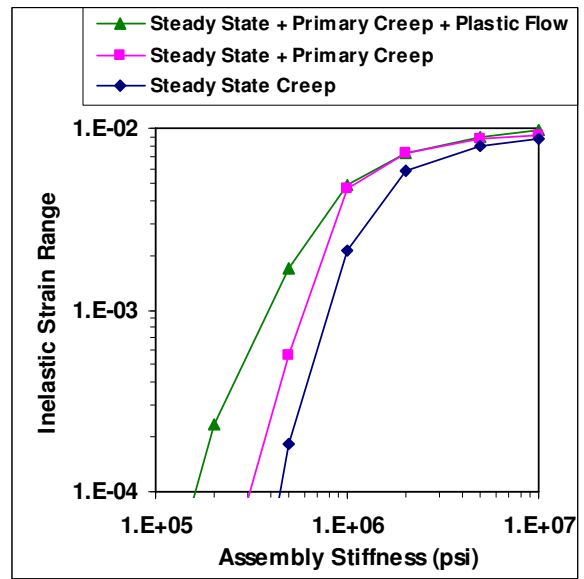Figure 25. Effect of constitutive relations on Inelastic Strain Range for 96.5Sn3.5Ag solder under temperature cycle condition 4 (0C⇔100C, 600 sec ramps, 300 sec dwells) and 1.0E-4/C imposed strain.

8. DISCUSSION

The present analysis has shown that thermal cycle acceleration factors depend on several factors: 1) imposed strain, 2) assembly stiffness and 3) solder properties. This has ramifications with respect to product qualification because the industry uses a common set of tests to qualify product. Unfortunately, it is probably not practical to tailor qualification tests to assembly stiffness or solder alloy type.

The magnitude of calculated acceleration factors also depends on the damage indicator that is chosen, i.e., strain range vs. strain energy density. The analysis community is somewhat polarized on this issue. People have their preference for using either strain range or strain energy density. The preference is usually based on historical practice within a company, believed theoretical "correctness", or academic lineage.

Based on the current analysis, it is clear that changing temperature cycling conditions is a good way to delineate which method gives the most accurate prediction. For example, it is expected that increasing ramp rate will reduce fatigue life based on strain energy density considerations, but have little effect on fatigue life based on strain range considerations. In reviewing the measured data in refs [35-36], fatigue life did decrease when ramp rate was increased significantly. This would tend to support strain energy density as a better damage indicator.

Solder alloy properties also have an impact on thermal cycle acceleration factors. Life predictions using strain range are more sensitive to variations in constitutive relations than those using strain energy density. Hence, it would follow that strain energy density is a more robust damage indicator.

9. CONCLUSIONS

1) The impact of assembly stiffness and solder properties on thermal cycle acceleration factors was investigated using a simplified model of an electronic assembly.

2) Stress – strain hysteresis loops change dramatically with modest changes in the assembly stiffness or the imposed strain.

3) The impact on strain range and strain energy density saturates as the assembly stiffness significantly exceeds that of the solder.

4) The acceleration factors between various temperature cycle conditions vary with assembly stiffness and solder

properties. Hence, standard qualification tests do not accelerate all types of surface mount components equally.

5) Strain energy density appears to be a more robust damage indicator than strain range, based on its lower sensitivity to specific constitutive relations.

10. REFERENCES

1] R. Subrahmanyan, D. Stone, and C.-Y. Li, "Deformation Behavior of Leadless 60Sn40Pb Solder Joints," Proceedings MRS Symposium, Vol 108, 1988, pp.381-384.

2] J. Sauber and J. Seyyedi, "Predicting Thermal Fatigue Lifetimes for SMT Solder Joints," Trans. ASME Journal of Electronic Packaging, Vol. 114, December 1992, pp. 473-476.

3] R. Darveaux and K. Banerji, "Fatigue Analysis of Flip Chip Assemblies Using Thermal Stress Simulations and a Coffin-Manson Relation," Proc. 41st IEEE ECTC, 1991, pp. 797-805.

4] B.N. Agarwala, "Thermal Fatigue Damage in Pb-In Solder Interconnections", International Reliability Physics Symposium, 1985, pp. 198-205.

5] R. Satoh, K. Arakawa, M. Harada, and K. Matsui, "Thermal Fatigue Life of Pb-Sn Alloy Interconnections," IEEE Trans. CHMT, Vol. 14, No. 1, March 1991, pp. 224-232.

6] Y. Uegai, S. Tani, A. Inoue, S. Yoshioka, and K. Tamura, "A Method of Fatigue Life Prediction for Surface-Mount Solder Joints of Electronic Devices By Mechanical Fatigue Test," Proc. ASME International Electronic Packaging Conference, 1993, Vol 1, pp. 493-498.

7] J.P. Clech and J.A. Augis, "Engineering Analysis of Thermal Cycling Accelerated Tests for Surface-Mount Attachment Reliability Evaluation," Proc. 7th IEPS, 1987, pp. 385-410.

8] A. Schubert, R. Dudek, E. Auerswald, A. Gollhardt, B. Michel, and H. Reichl, "Fatigue Life Models for SnAgCu and SnPb Solder Joints Evaluated by Experiments and Simulation," Proceedings 2003 ECTC, s14p6C, pp. 603-610.

9] A. Perkins and S.K. Sitaraman, "Thermo-Mechanical Failure Comparison and Evaluation of CCGA and CBGA Elecronic Packages," Proc. 2003 ECTC, pp. 442-430.

10] A. Syed, "Accumulated Creep Strain and Energy Density Based Thermal Fatigue Life Prediction Models for SnAgCu Solder Joints," Proceedings ECTC 2004, s16p7, pp. 737-746.

11] W. Engelmaier, "Functional Cycles and Surface Mounting Attachment Reliability," ISHM Technical Monograph Series 6984-002, International Society for

Hybrid Microelectronics, Silver Springs, MD, October 1984, pp. 87-114.

12] J-P. Clech, D.M. Noctor, J.C. Manock, G.W. Lynott, and F.E. Bader, "Surface Mount Assembly Failure Statistics and Failure Free Time," Proc. 44th IEEE ECTC, 1994.

13] J-P. Clech, J.C. Manock, D.M. Noctor, F.E. Bader, and J.A. Augis, "A Comprehensive Surface Mount Reliability (CSMR) Model Covering Several Generations of Assembly Technology," Proc IEEE 43rd ECTC, 1993, pp.62-70.

14] V. Sarihan, "Energy-Based Methodology for Damage and Life Prediction of Solder Joints under Thermal Cycling," Proc. IEEE 43rd ECTC, 1993.

15] R. Darveaux, K. Banerji, A. Mawer, and G. Dody, "Reliability of Plastic Ball Grid Array Assembly," Ball Grid Array Technology, J. Lau Editor, McGraw-Hill, Inc., New York, 1995.

16] R. Darveaux, "Optimizing the Reliability of Thin Small Outline Package (TSOP) Solder Joints," Advances in Electronic Packaging 1995 - Proc. ASME Interpack '95, pp. 675-685.

17] R. Darveaux, "Effect of Simulation Methodology on Solder Joint Crack Growth Correlation and Fatigue Life Prediction," Journal of Electronic Packaging, Vol 124, September 2002, pp. 147-154.

18] J-P. Clech, "Acceleration Factors and Thermal Cycling Test Efficiency for Lead-Free Sn-Ag-Cu Assemblies," Proc. SMTAI 2005.

19] J.H.L. Pang, P.T.H. Low, B.S. Xiong, "Lead-Free 95.5Sn-3.8Ag-0.7Cu Solder Joint Reliability Analysis for Micro-BGA Assembly," Proceedings 2004 ITHERM, pp.131-136.

20] J. Lau, W. Dauksher, and P. Vianco, "Acceleration Models, Constitutive Equations, and Reliability of Lead-Free Solders and Joints," Proceedings 2003 ECTC, s05p7C, pp. 229-236.

21] J-P. Clech, "An Obstacle-Controlled Creep Model for Sn-Pb and Sn-Based Lead-Free Solders," Proceedings 2004 SMTA International, pp. 776-802.

22] J-P. Clech, "An Extension of the Omega Method to Primary and Tertiary Creep of Lead-Free Solders," Proc. 2005 ECTC, pp. 1261-1271.

23] J.H.L. Pang, B.S. Xiong, and T.H. Low, "Creep and Fatigue Characterization of Lead Free 95.5Sn-3.8Ag-0.7Cu Solder," Proceedings 2004 ECTC, s30p4, pp. 1333-1337.

24] S. Wiese, M. Roellig, and K-J. Wolter, "Creep of Eutectic SnAgCu in Thermally Treated Solder Joints," Proc. 2005 ECTC, pp. 1272-1281.

25] R. Darveaux and K. Banerji, "Constitutive Relations for Tin Based Solder Joints," Proceedings IEEE 42nd ECTC, 1992, pp. 538-551, and IEEE Trans on CHMT, Vol. 15, No. 6, December 1992, pp. 1013-1024.

26] R. Darveaux, "Effect of Simulation Methodology on Solder Joint Crack Growth Correlation," Proc 2000 ECTC, pp. 1048-1058.

27] R. Darveaux and I. Turlik, "Shear Deformation of Indium Solder Joints," IEEE Transactions on Components, Hybrids, and Manufacturing Technology, Vol 13, No 4, December 1990, pp. 929-939.

28] R. Darveaux and K.L. Murty, "Effect of Deformation Behavior on Solder Joint Reliability Prediction," Proc. TMS-AIME Symposium, November 1992.

29] S.B. Park, R. Joshi, and L. Goldmann, "Reliability of Lead-Free Copper Columns in Comparison with Tin-Lead Solder Column Interconnects," Proc. 2004 ECTC, pp.82 - 89.

30] R. Darveaux and A. Syed, "Reliability of Area Array Solder Joints in Bending," Proc 2000 SMTAI, pp.313-324.

31] R. Darveaux, J. Heckman, and A. Mawer, "Effect of Test Board Design on the 2nd Level Reliability of a Fine Pitch BGA Package," Proc SMI 1998, pp. 105-111.

32] R. Darveaux, J. Heckman, A. Syed, A. Mawer, "Solder Joint Fatigue Life of Fine Pitch BGAs – Impact of Design and Material Choices," Microelectronics Reliability, Vol 40, 2000, pp. 1117-1127.

33] K.C. Norris and A.H. Landzberg, "Reliability of Controlled Collapse Interconnections", IBM Journal of Research and Development, May 1969, pp. 266-271.

34] R. Darveaux, "Shear Deformation of Lead Free Solder Joints," Proc. 2005 ECTC, pp. 882-893.

35] X. Fan, G. Raiser, and V.S. Vasudevan, "Effects of Dwell Time and Ramp Rate on Lead-Free Solder Joints in FCBGA Packages," Proc. 2005 ECTC, pp. 901-906.

36] A. Syed, T. Panczak, R. Darveaux, S.G. Lee, C.H. Lee, J. Partridge ,"Solder Joint Reliability of Chip Array BGA™," Proc. SMTA, 1999, pp. 90-97.